AIAA SciTech Forum
6-10 January 2025, Orlando, FL
AIAA SCITECH 2025 Forum

10.2514/6.2025-0823

Deep-learning-based Optimization of Non-periodic Porous and Composite Materials for Aerospace Structures

Saltuk Yıldız*, Zekeriya Ender Eğer†, and Pınar Acar‡
Virginia Tech, Blacksburg, 24061, VA, USA

In this study, a deep learning-based computational design framework is presented to optimize structures with non-periodic random inclusions and dual-phase materials. The dual-phase material is defined as a carbon fiber-reinforced polymer (CFRP) considering the low-weight requirements in aerospace applications. Additive manufacturing techniques allow the design flexibility for these materials to generate complicated topologies with enhanced mechanical performance. In the dual-phase composite, the optimal fiber locations are determined by minimizing the high stress/strain concentrations under complex loading involving tension and shear. On the other hand, the porous structure, which only includes the matrix polymer (i.e., without fibers), is studied to find the optimal locations of circular voids by minimizing the high stress/strain concentrations over the design domain. The locations of fibers and voids are randomly sampled to generate 450 geometries for each case, and the finite element method (FEM) is applied to these samples to create training and test data for a deep learning model. The main objective of the optimization is defined as the minimization of the energy fraction (E_f), which is selected as a metric of high stress/strain concentrations as it refers to the ratio of the strain energy density (W_e) of finite elements to the total strain energy density (W_{total}). The strain energy density function is formulated considering both tensile and shear force effects. The designs providing the minimum value of the maximum and average energy fractions are identified by integrating the optimization into the deep learning model.

Nomenclature

E	=	modulus of elasticity
E_f	=	energy fraction
W_e	=	strain energy density function
W_{total}	=	total strain energy density function
d_{rel}	=	relative density
t	=	layer thickness
u_{ii}	=	normal displacement
u_{ij}	=	shear displacement
x	=	x-coordinate
y	=	y-coordinate
σ_{ij}	=	stress
ε_{ij}	=	strain
ν_{ij}	=	Poisson's ratio

I. Introduction

Carbon fiber-reinforced polymers (CFRP) are widely used for aircraft structures such as fuselage, wings, tails, and the structure of unmanned aerial vehicles (UAVs) owing to their high strength-to-weight ratio. On the other hand, porous structures are commonly used in aerospace components due to their lightweight and outstanding mechanical behavior. These structures have become attractive with the enhancement of the 3D-printing techniques enabling the manufacturing of complex topologies [1]. Fused Filament Fabrication (FFF) is one affordable and common rapid

*Graduate Research Assistant, Ph.D. Student, Department of Mechanical Engineering, AIAA Student Member
†Graduate Research Assistant, Ph.D. Student, Department of Mechanical Engineering, AIAA Student Member
‡Associate Professor, Department of Mechanical Engineering, AIAA Member

prototyping method that uses the matrix and fiber material filaments to deposit molten material layer-by-layer on the build plate [2]. 3D-printing can easily handle non-homogeneous distributions of the inclusions either as dual-material or porous [3]. It might be challenging to model and optimize the non-periodic distributions, which require evaluation through efficient computational techniques to prevent possible mechanical failures in aerospace components [4–6]. The proper mathematical model development is required to predict non-homogeneous inclusion distributions to improve mechanical performance [7].

In an early study, Orozco and Pindera [8] proposed an efficient analysis called 'Generalized Method of Cells' to extract plastic properties of the composite material, where the unidirectional fibers were distributed randomly. Davis et al. [9] derived a mathematical model to determine elastic strain energy between any two adjacent rigid fibers in the 2D design domain neglecting their location under hydrostatic deformation. In addition to the elastic response predictions, the plastic deformation of composites having random inclusions is critical for the materials under extreme mechanical loading. In this regard, Ostoja-Starzewsk et al. [10] developed a numerical approach to simulate crack propagation along with local stress and strain distributions in a dual-phase material having randomly distributed inclusions. Al-Ostaz et al. [11] presented a correlation between random dispersion of the circular-shaped fibers and local stress fields for the microstructure of inclusion–matrix composites. They used Voronoi cell and Delaunay triangulation methods to quantify microstructures. The effective properties of materials having random entities can be extracted by modeling them as representative volume elements (RVEs). The elastic properties of a random non-homogeneous material were extracted by Ye and Yu [12]. They characterized the random distribution through a probability density function (PDF) and conducted the Maximum Entropy Method (MEM) to determine possible distributions of entities. Schneider et al. [13] carried out an efficient mesh generation approach to simulate 3D microstructures of randomized matrix-inclusion RVEs, preventing overlap. Acar et al. [14] optimized the fiber paths to minimize stress concentrations for a four-layer symmetric laminate and selected energy fraction as an objective function. Islam et al. [15] proposed a computational framework for the dual-phase material with random cylindrical fibers. Their method combined the Random Sequential Adsorption (RSA) and Finite Element (FE) methods.

Recently, data-driven methods such as machine and deep learning approaches have been proposed for efficient modeling and optimization of random distributions of the inclusions for enhanced mechanical performance. For this purpose, Ye et al. [16] created data sets from the microstructure images and finite element analysis (FEA), and trained them using a convolutional neural network (CNN) to determine the effective elastic properties such as modulus of elasticity and Poisson's ratio of homogenized composites with random shapes. Later on, Yang et al. [17] applied an image-based data-driven method called conditional generative adversarial neural network (CGAN) to predict the stress-strain behavior of the dual-phase microstructure. Recently, Rezasefat and Hogan [18] have conducted multi-decoder CNN (MUDE-CNN) and MUDE-CNN with transfer learning (MTED-TL) to efficiently predict time-dependent stress distributions along a 3D single circular pore located at the center of a cubic RVE. Sepasdar et al. [19] developed an image-based deep learning method (i.e., CNN) to predict non-linear stress distribution and deformation patterns. They generated 4500 data samples through FEA to train a neural network model, which achieved 90% accuracy [19]. Bhadury et al. [20] developed a statistical prediction method through CNN to determine local von Mises stress distributions on fiber-reinforced composites under uniaxial tension while considering that the structure involved a large number of random fibers. However, a systematic and efficient optimization for these structures under complex loading is still an open research topic in the literature. For instance, Saha et al. [21] predicted stress and strain maps for a composite material having circular random fibers under shear and tension using the U-Net method. However, a generalized design strategy that can be integrated to optimize the topology of both porous and composite materials is required.

CFRPs are typically composed of carbon fibers and a polymer matrix. The mechanical response of these materials is influenced by various design parameters including fiber shape, relative density, matrix shape, and fiber dispersion. The design variables can similarly be defined for the porous structures. In this study, a comprehensive and efficient computational and data-driven method is presented to determine the optimal locations of inclusions and voids under the complex loading assumption for the first time in the literature. A dual-phase material having uni-directional fibers, and a porous material having uni-directional pores in two dimensions are studied to determine optimum fiber and porosity locations using a deep-learning-based surrogate model. Porous and CFRP materials are simulated under shear and tension through FEA. The location dispersions of circular fibers and pores, defined as the inputs of the deep learning model, are generated through uniform random distributions. Next, FEA simulations are performed for these geometries to produce the outputs of the deep learning model, involving feed-forward neural network (FNN). A design optimization framework is presented to determine optimal geometries leading to minimum energy fractions for non-periodic porous and dual-phase composite materials. The presented model is cost-effective over existing approaches with the integration of deep learning. The expected mechanical performance improvement for the low-weight composites and porous

structures in this study is anticipated to increase their use in aerospace industry applications.

The outline of the study is as follows. In Section 2, the computational modeling of porous and composite structures and the FEA setup are explained. In the following sections, the deep-learning model and the optimization strategy are presented.

II. Methodology

A. Computational modeling of design domain

In this study, an iterative computational design model is developed to generate porous and dual-phase materials with randomly distributed void and inclusion distributions, respectively. For this purpose, the computational domain is generated with 5000×5000 pixels, which provides a high-quality representation of circular shapes. Next, 4 circles having random x and y center coordinates are deleted from the domain to create the secondary phase, where the coordinates are located using a random uniform distribution. The non-periodic inclusion phases for porous and composite materials are demonstrated in Fig. 1.

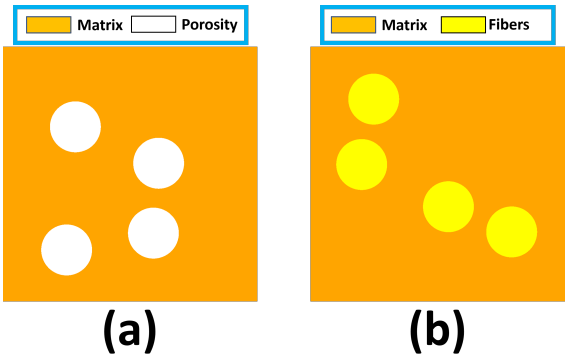

Fig. 1 Computational design of non-periodic (a) porous and (b) composite material.

In the design framework, a large number of synthetic samples are generated. There are 4 circles ($n = 4$) designed iteratively having randomized locations starting with ($k = 0$) (see Fig. 2). In the design algorithm, center locations are limited by the domain boundary, and the distance between the center locations of circles is selected as 1.2 times the diameter value to prevent overlap between circles and a possible mesh generation problem between inclusions.

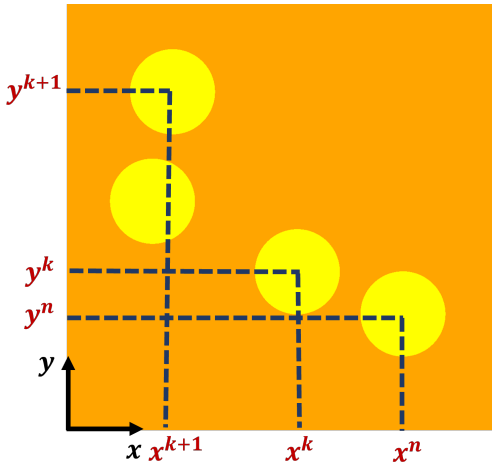

Fig. 2 Random fiber locations.

As seen from Fig. 2, circles are generated iteratively, and design constraints are checked in each iteration. Each

design has some constant features such as side lengths (δ_x and δ_y), circle diameter (d), the minimum distance between circles (d_{min}), and the number of circles (N), etc. These constant features are demonstrated in Fig. 3.

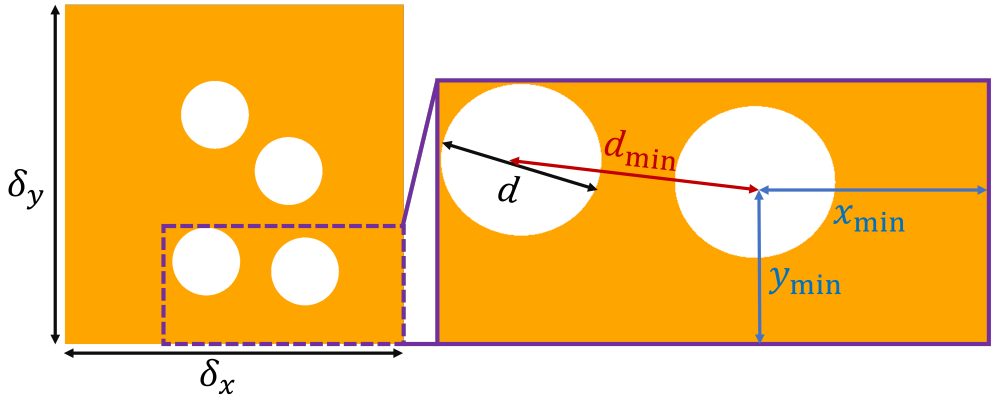

Fig. 3 Geometric features defined in the algorithm.

In addition, x_{min} and y_{min} are the minimum distances between circle center locations and domain boundaries in x and y directions, respectively, d_{rel} stands for relative density, which is the ratio of the matrix material area to the overall domain area. The fixed geometric parameters of the materials are listed in Table 1.

Table 1 Geometric parameters.

Parameter	Value
δ_x (in mm)	5
δ_y (in mm)	5
d (in mm)	1
d_{min} (in mm)	1.2
x_{min} (in mm)	1
y_{min} (in mm)	1
d_{rel} (%)	87
N	4

450 design samples are generated for both composite and porous materials to meet the data requirement of the deep-learning model. Some example designs are demonstrated in Fig. 4.

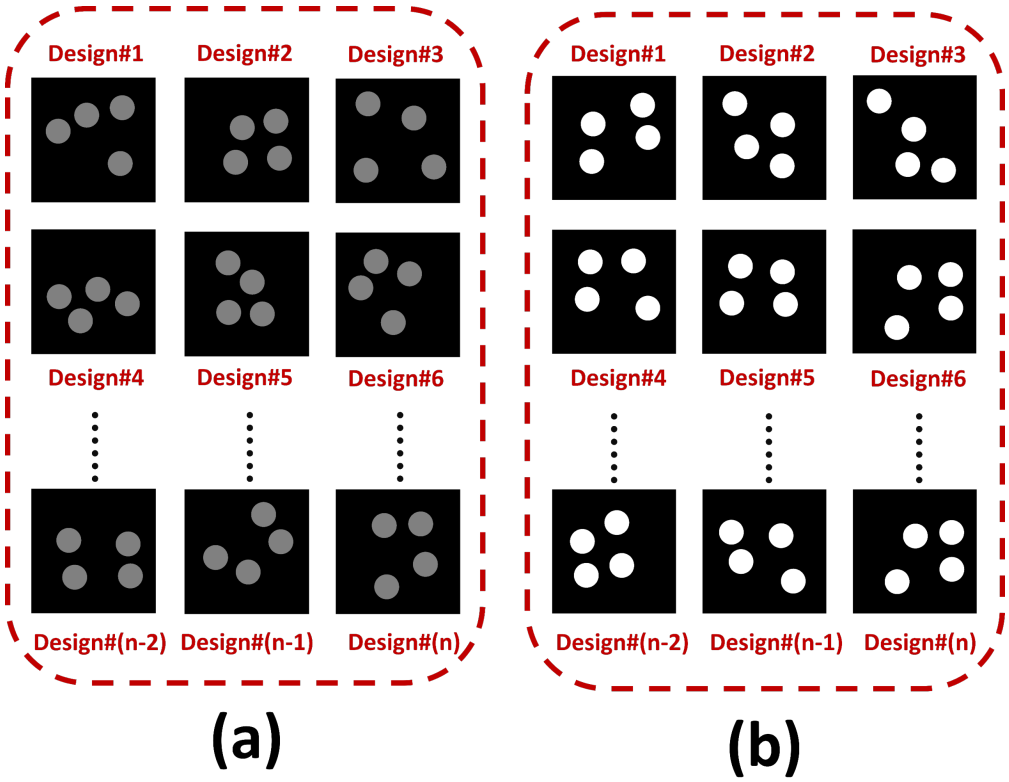

Fig. 4 Example input geometries created for (a) composite and (b) porous materials.

B. Finite element analysis for mechanical performance

In this section, the average directional stress and deformation values are extracted from FEM calculations including all stress and strain component values. The domain involves a 2D homogeneous solid under the plane stress assumption. The elemental (W_e) and total (W_{total}) strain energy density functions are calculated using Eqs. (1) and (2), respectively where M represents the total number of mesh elements.

$$W_e = \frac{1}{2} \sum_{i=1}^{N=2} \sum_{j=1}^{N=2} \sigma_{ij} \cdot \varepsilon_{ij} \tag{1}$$

$$W_{total} = \sum_{e=1}^{M} W_e \tag{2}$$

The energy fraction (E_f), which is used in the objective function of the optimization problem, is determined by the ratio of strain energy density to the total strain energy density as shown in Eq. (3)

$$E_f = W_e / W_{total} \tag{3}$$

The definition of the elastic material model in numerical simulation is acquired from the literature. The elastic properties of the FFF printed CFRP material are provided in Table 2 using the data from Ref. [3].

Table 2 Elastic properties of an additively manufactured CFRP [3].

Property	Carbon Fiber	Nylon Matrix
Modulus of elasticity, E (in MPa)	85,000	380
Poisson's ratio, ν_{12}	0.3	0.35

The geometries are created as gray-scale binary images, and imported as inputs to the MATLAB. Next, the im2mesh function [22], which refines the elements at the locations of high curvatures, is utilized to generate triangular finite element meshes. A static structural FEA is carried out using ABAQUS/Standard software. In FEA, around 170,000 grids for dual-phase geometries, and 140,000 elements for porous materials are used with the three-node plane stress element (CPS3), which provides convergent static structural simulations. The detailed representation of the meshed domains is illustrated in Fig. 5.

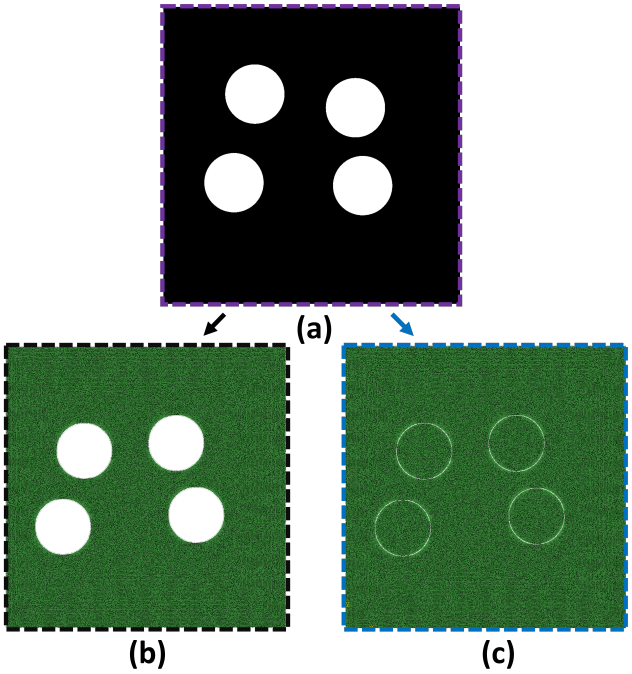

Fig. 5 Mesh generation for a (a) gray-scale image of (b) porous and (c) composite materials [22].

The designs are simulated under uni-axial tension and shear, where the geometry is considered as fixed at the bottom along x and y directions. The displacements (u_{ii} and u_{ij}) are applied as tension and shear with the values of 20% of the size of the domain. The boundary condition defined for the computational domain is depicted in Fig. 6. The linear elastic material model is used in the structural analysis.

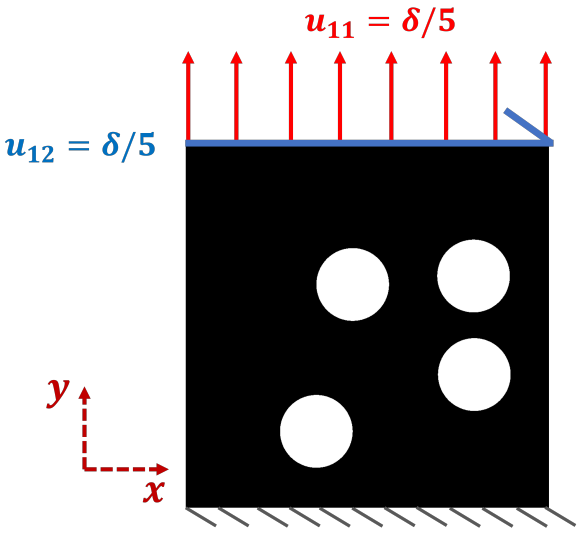

Fig. 6 Boundary and complex displacement conditions.

III. Deep Learning-based Surrogate Model for FEA

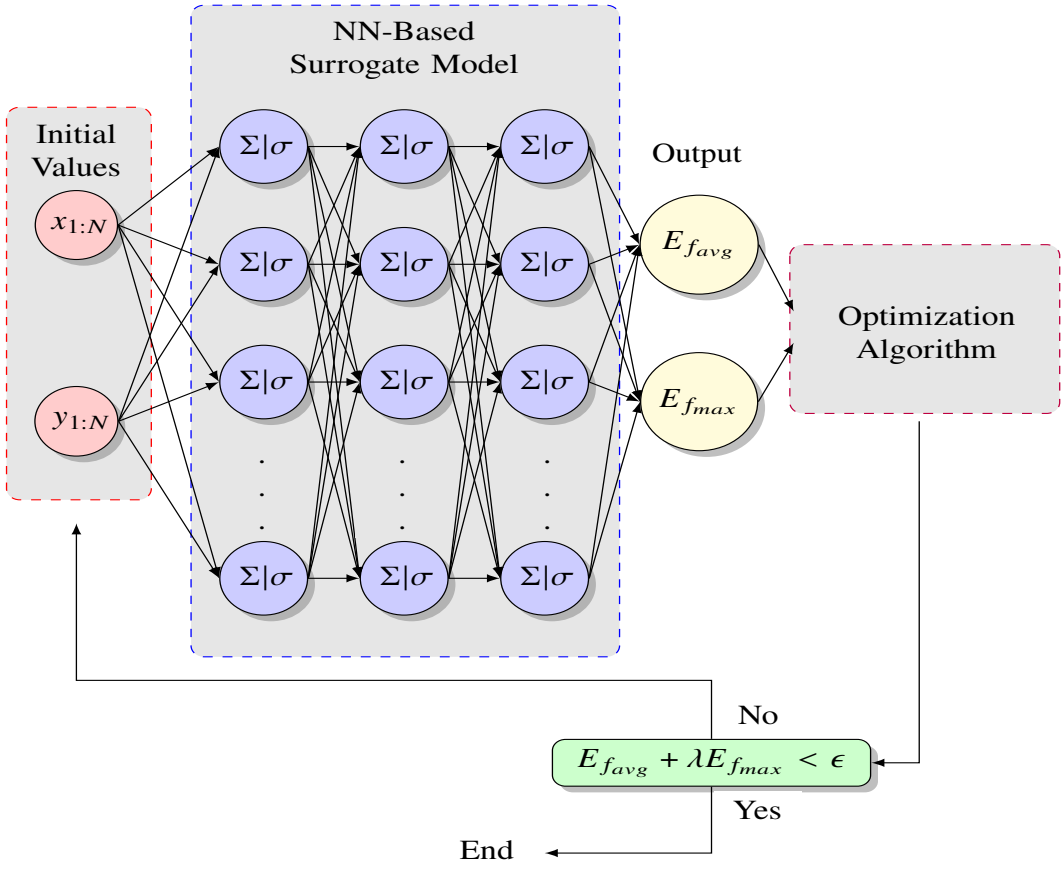

Fig. 7 Schematic of the surrogate model framework. The network will be trained with the variables in the design space to predict the $E_{f_{avg}}$ and $E_{f_{max}}$ parameters and then used to minimize the objective function.

To replace time-consuming simulations, a framework for a neural network-based surrogate model is developed, as illustrated in Fig. 7. This model is specifically designed to support optimization processes, which require many iterations and would be impractically slow if run with the full simulation model at each step. The surrogate model development begins with storing simulation inputs and outputs, representing the coordinates of circle centers and the maximum and average values of E_f, respectively. To compute the average value of E_f, only values exceeding a threshold based on the baseline design are included. Energy fraction values are calculated for 450 different configurations of dual-phase and porous materials using the FEA outputs. Some elemental E_f results are given in Fig. 8. A threshold value for energy fractions is determined, and the energy fractions that exceed the threshold for corresponding elements are counted to determine design configurations with more susceptibility to structural damage. From the 450 generated data points, a 350-50-50 split is applied for training, validation, and testing. Data generation takes an average of 1.1449e+05 and 1.6949e+05 seconds on a cluster with an AMD EPYC 7702 CPU clocked at 3.35 GHz for porous and composite materials, respectively.

The neural network architecture is optimized to balance performance and efficiency, ultimately settling on a simple feed-forward network with three layers of 128 neurons, using ReLU activations and 10 % dropout. Larger architectures are found to provide no additional accuracy, while smaller ones result in longer training times. Due to the compact learning space with 8 input parameters and 2 outputs, training is completed in only a few seconds. The model achieves similar mean absolute error (MAE) values for both validation and test sets, with MAE values of 7.91 % for the porous model and 8.31 % for the composite model. As a result, the average fit is found to be better than the maximum fit, likely due to mesh-based limitations, which can introduce unexpected jumps in maximum value calculations [23].

Despite these achievements, the scarcity of data prevents further reduction in the MAE. Nevertheless, this surrogate model offers a fast, practical, and sufficiently accurate alternative to iterative optimization, as shown by the comparison of actual and predicted values on test data for both maximum and average E_f values in Fig. 9.

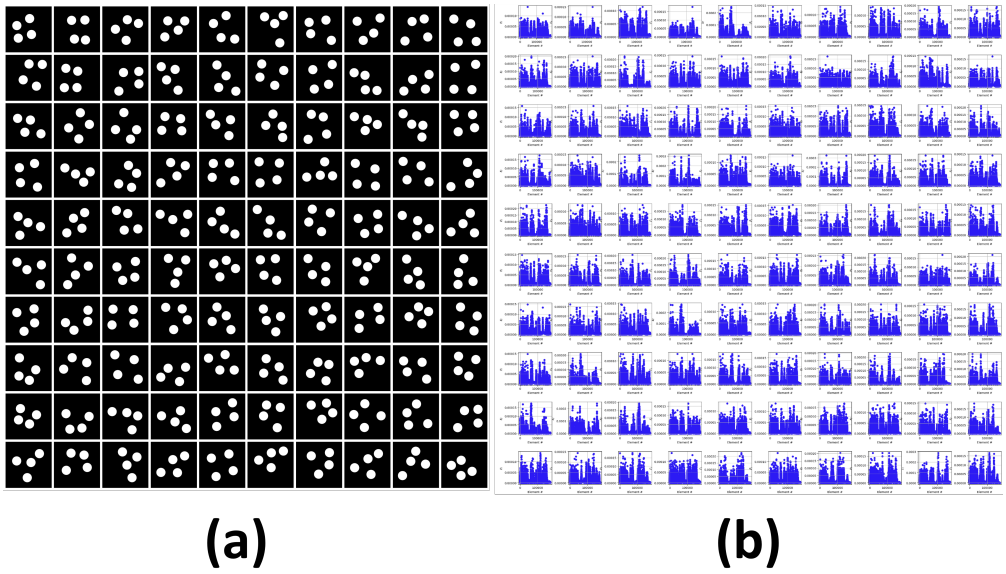

Fig. 8 Sample geometry and energy fraction data generated for the porous material.

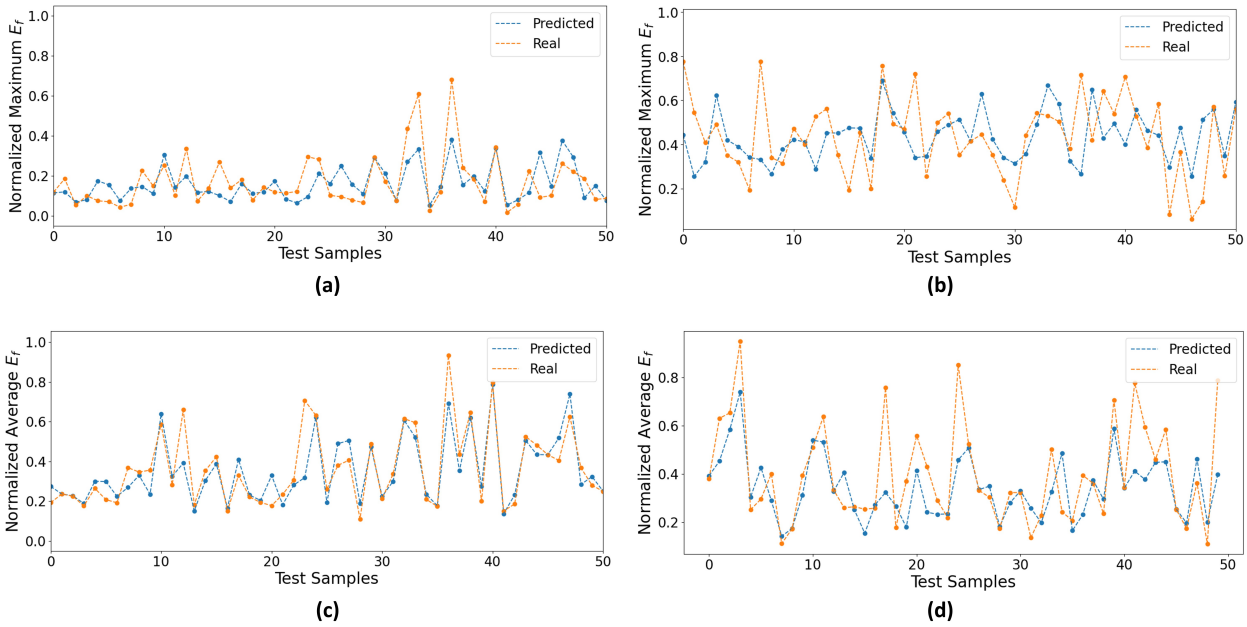

Fig. 9 Performance of the surrogate model on the test data for maximum $E_{f_{max}}$ predictions of (a) porous (b) composite materials, and for average $E_{f_{avg}}$ predictions of (c) porous (d) composite materials.

IV. Optimization of Porous and Composite Material Design

An optimization framework is developed to determine the optimum values of the center coordinates (i.e., x and y values) for the inclusions and voids of the composite and porous materials, respectively, to minimize a composite objective function of E_{fmax} and E_{favg} values under 3 design constraints ensuring that the fibers or voids are within the domain boundary without any geometric overlap. The optimization formulation is given in Eq. 4. The number of circles is represented by N and λ is the coefficient to adjust the weight in the objective function. The distance between the circles is denoted as d and d_{min} is the minimum value of that distance can be assigned to. δ shows the length of the design domain in both directions.

$$\begin{aligned} &\text{find} && x_k, y_k \\ &where && k = 1, 2, ..., N = 4 \\ &\text{minimize} && E_{f_{avg}} + \lambda \times E_{f_{max}} \\ &\text{subject to} && d \leq x \leq \delta_x - d, \\ & && d \leq y \leq \delta_y - d, \\ & && d_{\min} = d \times 1.2 \end{aligned} \tag{4}$$

The pattern search algorithm, which is a derivative-free optimization method, is chosen due to its ability to work without gradient computations [24]. This is a critical feature given that the FE model's output space is highly irregular for certain design points, with numerous peaks and non-smooth regions. In this algorithm, optimization begins with an initial guess and a step size, exploring a pattern of points around the current solution by incrementally adjusting each variable. If a better solution is found, the algorithm may increase the step size to explore further in that direction; if not, it reduces the step size, refining the search in smaller steps. This pattern of exploration and step-size adjustment continues until a convergence criterion is met, typically when the step size is minimal or improvements stop. To ensure a fair comparison of the optimization results, the pattern search algorithm is applied to both FE and surrogate models. It must be pointed out that even though the pattern search algorithm is less likely to converge a local solution, compared to gradient-based optimization, the selection of the initial points is still important for accuracy and computing time efficiency. The optimization is completed in the scale of only a few seconds when using the surrogate model where it takes about 7.4331e+05 seconds when using the FE model on average, showing the immense computational expense.

V. Results & Discussions

The maximum and average energy fractions of the porous and composite materials are minimized by finding the optimal center locations of circular-shaped fibers and void phases by integrating optimization into FE (physics-based) and FNN (deep-learning) models. The λ parameter in Eq. 4 is set to 0.66 in order to negate the scale difference between expected output values. The results for both models for the porous material are presented in Fig. 10. The outputs are very similar, and the error is calculated using the Euclidean distances between the points, where the maximum distance is taken as the distance from corner to corner inside the bounds. The errors are found to be 5.61%, 5.18 %, 0.12 %, and 1.64 % for each of those four points. This, along with the visual similarity of outputs, suggests that the surrogate model effectively captures the behavior of the porous materials. When the optimum design found with the surrogate model is used to calculate the $E_{f_{avg}}$, the error is found to be 14.7 %. Furthermore, the fact that the deep-learning output can be used as the initial point for optimization with the physics-based model is highly promising, as it will greatly reduce computational times.

The same procedure is repeated for the composite material, and the errors are found to be 21.39 %, 7.73 %, 2.41%, and 7.49 % for each point. For the $E_{f_{avg}}$, the error is found to be 6.1 %.

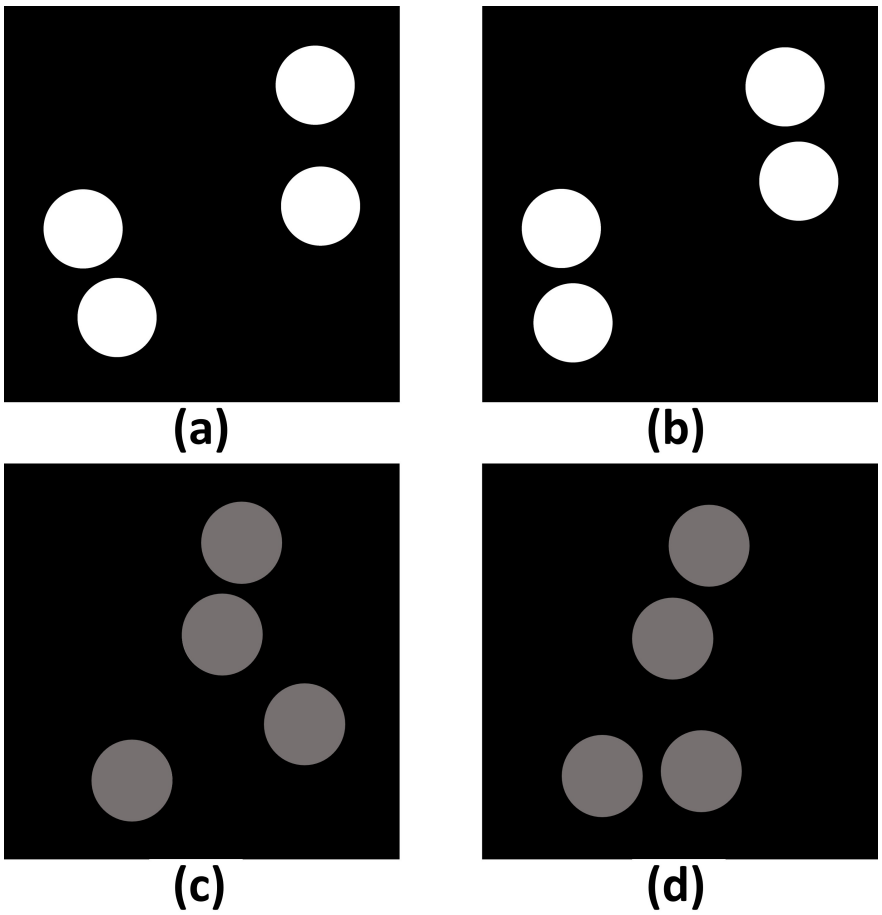

Fig. 10 Optimization results obtained using (a) FNN (deep-learning) (b) FE (physics-based) models for the porous material. In a similar fashion, the results for the composite material are shown for (c) FNN (deep-learning) (d) FE (physics-based) models.

Figure 11 shows an exemplary contour plot of the stress (σ_{22}) and strain (ε_{22}) distributions over the computational domain of the porous structure for the baseline configuration, where the pores are distributed regularly, and the optimum design obtained by the FNN-based approach.

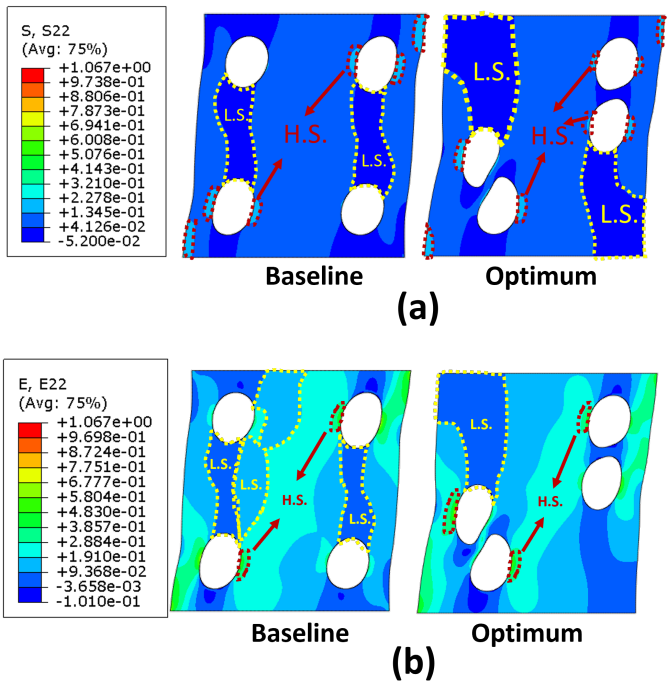

Fig. 11 FEA simulation results for baseline and optimum porous materials: (a) σ_{22} and (b) ε_{22} distributions. H.S. and L.S. stand for high-stress/strain and low-stress/strain regions, respectively.

As clearly seen from Fig. 11, optimum geometry reveals more dominant low-stress/strain regions in contrast with the baseline configuration. For the composite material, the differences in objective functions of the baseline, FNN-based, and FE-based optimum designs are shown in Fig. 12.

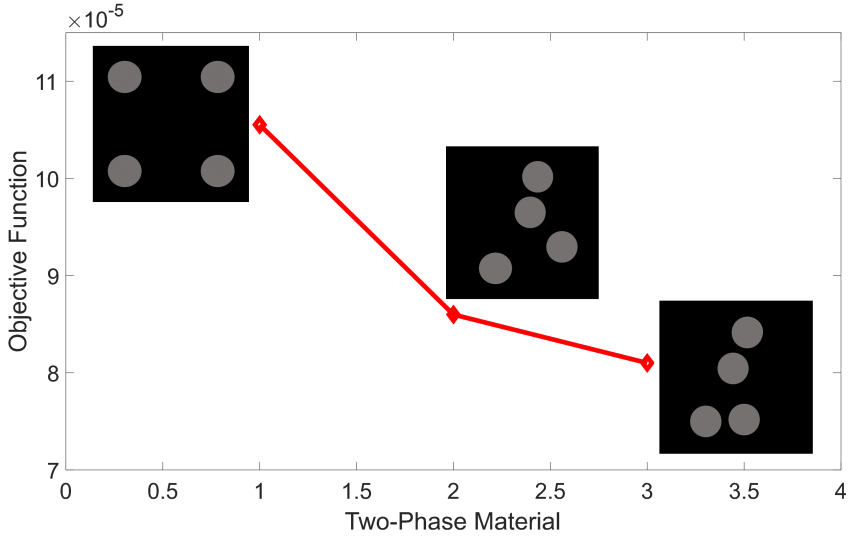

Fig. 12 Objective function comparison of baseline and optimized geometries for the two-phase composite material.

According to the objective function comparison, the optimization using the physics-based FE model identifies the best design, which has 23.2% mechanical performance improvement over the baseline configuration. On the other hand,

the FNN-based optimum result demonstrates 18.5% performance improvement, which is in good agreement with the FE-based result, while also improving computational time efficiency significantly.

VI. Conclusion

In this study, porous and CFRP materials under complex loading conditions including shear and tension loads are designed by optimizing the fiber and void phase distributions. First, a large number of data samples, involving material geometries and corresponding energy fraction values obtained from FEA, is created to train a neural network model. Later, a design optimization framework is developed to find optimal coordinates of the fibers and void phases in the design domain. The main purpose of the design optimization framework is to minimize the energy fraction, which is a selected metric of the high stress/strain concentrations. The optimization problem is solved with the pattern-search algorithm using both the FE and FNN models. According to the optimization results, the surrogate model achieves substantial mechanical performance improvements for lightweight composites and porous materials that can be used as aerospace structures while reducing computation times. The specific outputs of this computational work can be drawn as:

- The high stress/strain regions of linear elastic material are drastically reduced. The energy fraction criteria are utilized in both FNN-based and FE-based optimization as an objective function to carry out a quantitative evaluation of stress/strain distributions.
- A low-cost FNN-based prediction model is developed for two types of aerospace materials, which are porous and two-phase composite materials. This model is used for design optimization, where the optimum coordinates of pores and fibers are determined to improve mechanical performance.
- The FNN-based optimum designs for both materials are in good agreement with the optimum results of the FE-based solution. Therefore, the surrogate model based optimization can replace the time-consuming optimization solution via the FE-based approach.
- This deep-learning model can be generalized for different design cases of multi-phase materials involving different sizes of phases, domains, and geometry with higher numbers of pores/fibers. In addition, the model output can be used as an initial condition for the FE-based optimization to reduce excessive computational times.

Acknowledgments

The authors acknowledge the financial support from the National Science Foundation CAREER Award CMMI-2236947 and the Future Additive Interdisciplinary Manufacturing (FAIM) project supported under the National Defense Education Program of the Office of Naval Research (ONR).

References

[1] Sanei, S. H. R., and Popescu, D., "3D-printed carbon fiber reinforced polymer composites: a systematic review," *Journal of Composites Science*, Vol. 4, No. 3, 2020, p. 98.

[2] Górski, F., Wichniarek, R., Kuczko, W., and Andrzejewski, J., "Experimental determination of critical orientation of ABS parts manufactured using fused deposition modelling technology," *Journal of Machine Engineering*, Vol. 15, No. 4, 2015, pp. 121–132.

[3] Al Abadi, H., Thai, H.-T., Paton-Cole, V., and Patel, V., "Elastic properties of 3D printed fibre-reinforced structures," *Composite Structures*, Vol. 193, 2018, pp. 8–18.

[4] Zhu, D., and Wu, P., "Asymptotically analytical solution of elastic stress for convex polygonal holes in an infinite plane under various loading conditions," *Acta Mechanica*, Vol. 232, 2021, pp. 3957–3975.

[5] Rezasefat, M., Giglio, M., and Manes, A., "Numerical investigation of the effect of open holes on the impact response of CFRP laminates," *Applied Composite Materials*, Vol. 29, No. 4, 2022, pp. 1555–1578.

[6] Schmit, L. A., and Mehrinfar, M., "Multilevel optimum design of structures with fiber-composite stiffened-panel components," *AIAA journal*, Vol. 20, No. 1, 1982, pp. 138–147.

[7] Zhang, L., Chen, Z., Mao, J., Wang, S., and Zheng, Y., "Quantitative evaluation of inclusion homogeneity in composites and the applications," *Journal of Materials Research and Technology*, Vol. 9, No. 3, 2020, pp. 6790–6807.

[8] Orozco, C. E., and Pindera, M.-J., "Plastic analysis of complex microstructure composites using the generalized method of cells," *AIAA journal*, Vol. 37, No. 4, 1999, pp. 482–488.

[9] Davis, L., Hass, K., Chen, J., and Thorpe, M., "Elastic moduli of composites with random, rigid inclusions," 1994.

[10] Ostoja-Starzewski, M., Sheng, P., and Jasiuk, I., "Damage patterns and constitutive response of random matrix-inclusion composites," *Engineering Fracture Mechanics*, Vol. 58, No. 5-6, 1997, pp. 581–606.

[11] Al-Ostaz, A., Diwakar, A., and Alzebdeh, K. I., "Statistical model for characterizing random microstructure of inclusion–matrix composites," *Journal of materials science*, Vol. 42, 2007, pp. 7016–7030.

[12] Ye, Z., and Yu, W., "On homogenization of random heterogeneous materials," *51st AIAA/ASME/ASCE/AHS/ASC Structures, Structural Dynamics, and Materials Conference 18th AIAA/ASME/AHS Adaptive Structures Conference 12th*, 2010, p. 2978.

[13] Schneider, K., Klusemann, B., and Bargmann, S., "Automatic three-dimensional geometry and mesh generation of periodic representative volume elements for matrix-inclusion composites," *Advances in Engineering Software*, Vol. 99, 2016, pp. 177–188.

[14] Acar, P., Vijayachandran, A. A., Sundararaghavan, V., Waas, A., and Rassaian, M., "Optimization of spatially varying fiber paths for a symmetric laminate with a circular cutout under remote uniaxial tension," *SAE International Journal of Materials and Manufacturing*, Vol. 9, No. 1, 2016, pp. 75–80.

[15] Islam, M., Tudryn, G. J., and Picu, C. R., "Microstructure modeling of random composites with cylindrical inclusions having high volume fraction and broad aspect ratio distribution," *Computational Materials Science*, Vol. 125, 2016, pp. 309–318.

[16] Ye, S., Li, B., Li, Q., Zhao, H.-P., and Feng, X.-Q., "Deep neural network method for predicting the mechanical properties of composites," *Applied Physics Letters*, Vol. 115, No. 16, 2019.

[17] Yang, Z., Yu, C.-H., and Buehler, M. J., "Deep learning model to predict complex stress and strain fields in hierarchical composites," *Science Advances*, Vol. 7, No. 15, 2021, p. eabd7416.

[18] Rezasefat, M., and Hogan, J. D., "Prediction of 4D stress field evolution around additive manufacturing-induced porosity through progressive deep-learning frameworks," *Machine Learning: Science and Technology*, Vol. 5, No. 1, 2024, p. 015038.

[19] Sepasdar, R., Karpatne, A., and Shakiba, M., "A data-driven approach to full-field nonlinear stress distribution and failure pattern prediction in composites using deep learning," *Computer Methods in Applied Mechanics and Engineering*, Vol. 397, 2022, p. 115126.

[20] Bhaduri, A., Gupta, A., and Graham-Brady, L., "Stress field prediction in fiber-reinforced composite materials using a deep learning approach," *Composites Part B: Engineering*, Vol. 238, 2022, p. 109879.

[21] Saha, I., Gupta, A., and Graham-Brady, L., "Prediction of local elasto-plastic stress and strain fields in a two-phase composite microstructure using a deep convolutional neural network," *Computer Methods in Applied Mechanics and Engineering*, Vol. 421, 2024, p. 116816.

[22] Jiexian, M., "Im2mesh (2D image to triangular meshes)(https://www. mathworks. com/matlabcentral/fileexchange/71772-im2mesh-2d-image-to-triangular-meshes)," *MATLAB Central File Exchange*, 2021.

[23] Zienkiewicz, O. C., and Taylor, R. L., *The finite element method set*, Elsevier, 2005.

[24] Audet, C., and Dennis Jr, J. E., "Analysis of generalized pattern searches," *SIAM Journal on optimization*, Vol. 13, No. 3, 2002, pp. 889–903.